Engineering Structures 212 (2020) 110276

Contents lists available at ScienceDirect

Engineering Structures

journal homepage: www.elsevier.com/locate/engstruct

Surrogate SDOF models for probabilistic performance assessment of multistory buildings: Methodology and application for steel special moment frames

Shaghayegh Vaseghiamiri[a], Mojtaba Mahsuli[a], Mohammad Ali Ghannad[a], Farzin Zareian[b,*]

[a] Center for Infrastructure Sustainability and Resilience Research, Department of Civil Engineering, Sharif University of Technology, Tehran, Iran
[b] Department of Civil and Environmental Engineering, University of California – Irvine, Irvine, USA

ARTICLE INFO

Keywords:
Risk analysis
SDOF models
Collapse assessment
Bayesian linear regression
Steel special moment frame buildings

ABSTRACT

This paper proposes a methodology for generating surrogate single-degree-of-freedom (SDOF) models that can be utilized to estimate the probability distribution of the roof drift ratio of multistory buildings at various ground motion intensity measures. The use of an SDOF model as a surrogate for multistory buildings can significantly alleviate the high computational cost for probabilistic seismic demand assessment considering both model uncertainty and record-to-record variability. The surrogate SDOF model generated herein explicitly accounts for model uncertainties and can be used as an alternative to the nonlinear dynamic analysis of detailed building structures. Applications for such surrogate models include regional risk and resilience analyses and comprehensive parametric studies. To showcase the proposed methodology, an SDOF surrogate model for steel special moment frame (SMF) buildings is developed using the suggested surrogate SDOF model generating methodology. The properties of the surrogate model representing a multi-degree-of-freedom (MDOF) structure are computed using a probabilistic function of the fundamental period of the structure developed using Bayesian linear regression. To validate the surrogate model for SMFs, the response statistics produced using detailed multistory SMF models are compared with those of the corresponding surrogate SDOF models. The results show that the proposed surrogate SDOF model captures the probability distribution of the roof drift ratio of SMFs up to collapse with acceptable accuracy while reducing the runtime by at least one order of magnitude.

1. Introduction

Estimating the response statistics of building structures is one of the most important and computationally-intensive steps of regional risk and resilience analyses. It is computationally intensive given the large number of buildings that are used in such analysis. Moreover, the accuracy of the response predictions directly affects the accuracy of the resulting risk/resilience estimates as errors will propagate through the downstream consequence and recovery models. Both the issues of computational cost and error are exacerbated given the high nonlinearity of the behavior of structures under scenarios of severe earthquakes [1,2] that are of particular importance in risk and resilience analyses. For instance, such analyses need to model the collapse of structures as it markedly impacts the social and economic consequences, e.g., casualties and repair costs. This requires a reliable assessment of the nonlinear response of the building structures from linear elastic range through collapse with a comprehensive treatment of epistemic and aleatory uncertainties. Accordingly, alternative methods have been developed [1,3–5] to alleviate this computational cost. Among the widely used alternatives to the nonlinear dynamic analysis of detailed building models are the 'displacement coefficient method' [6] adopted by ASCE/SEI 41 [7] and the 'capacity spectrum method' [8] adopted by FEMA-NIBS loss estimation methodology and implemented in HAZUS [9]. More recently, a novel variation of the capacity spectrum method is also developed by Rossetto et al. [10], which uses inelastic spectra of real ground motion records. Both methods rely on spectral analysis of an equivalent single-degree-of-freedom (SDOF) system as a surrogate for multi-degree-of-freedom (MDOF) buildings to produce an estimate of the roof drift. Another alternative in the literature is the regression equations that directly compute the responses given the spectral acceleration and observable building characteristics, such as height [11,12]. The present paper proposes a novel approach to develop a surrogate SDOF model with a multi-linear back-bone curve that captures the response statistics of a detailed MDOF model of the

* Corresponding author.
E-mail addresses: mahsuli@sharift.edu (M. Mahsuli), ghannad@sharif.edu (M.A. Ghannad), zareian@uci.edu (F. Zareian).

https://doi.org/10.1016/j.engstruct.2020.110276
Received 16 July 2019; Received in revised form 11 January 2020; Accepted 21 January 2020
Available online 16 April 2020
0141-0296/

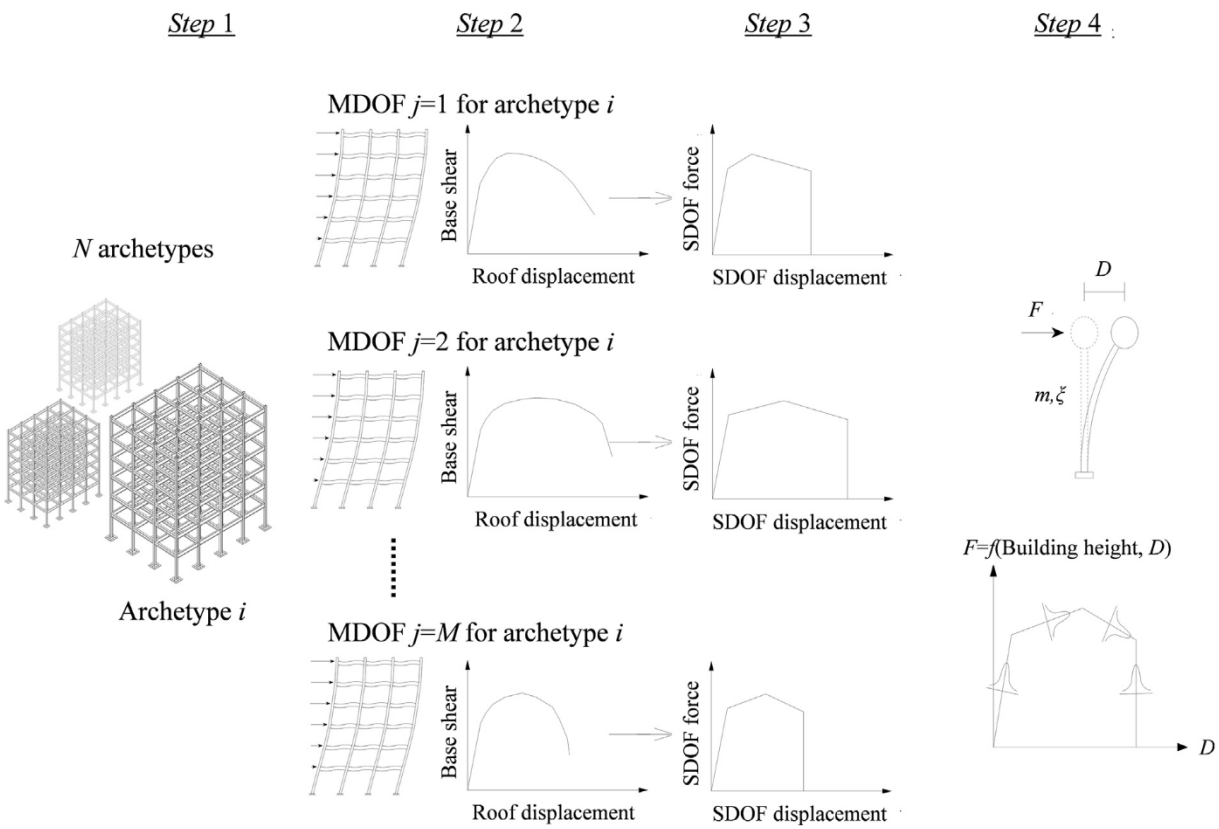

Fig. 1. Illustration of the four-step procedure.

building. Bayesian linear regression is employed to develop probabilistic models for computing the parameters of the backbone curve. The proposed surrogate model is shown to significantly reduce the computational cost of the probabilistic response analysis while exhibiting reasonable accuracy.

Analysis of building structures using SDOF models was first studied using bilinear spring models with negative post-elastic stiffness representing P-Δ effects [13,14]. Through the development of advanced hysteretic models, this seismic performance characteristic was assessed by incorporating strength and stiffness deterioration (monotonic and cyclic alike) in the hysteretic response of SDOF systems [15,16]. The effect of SDOF model parameters on the collapse capacity was extensively studied by [17]. The effect of cyclic and in-cycle degradation on the seismic response of different lateral systems was studied by FEMA P-440a [18] using SDOF models. These SDOF models were defined with a hysteretic model based on information available in the literature [19–23]. In these studies, record-to-record (RTR) variability was considered without incorporation of model uncertainty. However, studies on the combined effect of model uncertainty and RTR variability on the collapse capacity of building structures indicate that incorporating model uncertainty can significantly alter the estimates of the collapse capacity [24]. For example, Gokkaya et al. [2] showed that incorporating model uncertainty can shift the median and dispersion of collapse fragility curves up to 20% and 70%, respectively. Villar-Vega et al. [25] used sets of SDOF systems to develop fragility models for residential areas in South America by assuming the same level of uncertainty in all SDOF models. The use of simplified equivalent SDOF models in vulnerability assessment of buildings has also been addressed by GEM (Global Earthquake Model) [26]. Abthai et al. [27] proposed a relationship between the strength demands of MDOF systems with that of equivalent SDOF models with an elastic-perfectly-plastic nonlinear behavior considering prevailing uncertainties. Recently, several simplified procedures are proposed for incorporating model uncertainty in the collapse assessment of MDOF buildings [4,28,29,5], which mainly use pushover-based simplification to predict the collapse capacity.

In the research presented herein, a methodology is proposed for generating surrogate SDOF models that can mimic the response of MDOF systems up to the collapse state in a probabilistic context. This methodology is then used to generate surrogate models for steel special moment frame (SMF) structures. The probabilistic characterization of the backbone curve of the surrogate model is given for a practical range of SMF building heights. To develop the latter, pushover analyses are conducted on a set of multistory SMF building models generated according to model uncertainty in their basic component parameters. The pushover analysis is performed in accordance with the fundamental mode of vibration of buildings. Hence, there is an inherent assumption in the surrogate SDOF model that the dynamic response of the structure is mostly governed by the fundamental mode of vibration. However, it should be noted that SDOF models are generally advised in the literature for estimating drift ratios [30] and the effect of higher modes is more pronounced in other structural responses such as the base shear. In order to account for the uncertainty in design specifications, different SMF building archetypes are designed according to target seismic design codes. In fact, model uncertainty is taken into account by considering randomness in the properties of elements of the designed buildings. The distribution of the input parameters of the surrogate models is estimated by idealizing force-displacement relationship obtained from pushover analysis of the MDOF building models. The properties of the surrogate model are provided as a probabilistic function of the fundamental period of MDOF structures, developed using Bayesian linear regression [31]. Once the proposed probabilistic surrogate model is developed for a lateral load resisting system, no further nonlinear analyses at the level of MDOF structure is needed and users can solely rely on the surrogate model for seismic performance assessment. This technique is in contrast with the probabilistic equivalent SDOF model proposed by Kosič et al. [5], where a single pushover analysis is needed for each representative MDOF system considered in the probabilistic assessment of the collapse capacity.

The proposed methodology is limited to predicting the roof drift demand of building structures while ongoing research by the authors addresses other important responses, such as interstory drift and floor acceleration. In addition, the methodology presented herein is aimed at the regional analysis of a portfolio of buildings, and *not* at detailed risk analysis of a single building structure; it serves as an alternative to similar approximate methods, e.g., displacement coefficient method and capacity response spectrum. The proposed models can also be employed in studies that entail comprehensive parametric analysis of building structures, such as [24,32,33] among others.

2. Methodology

A four-step procedure is suggested – schematically illustrated in Fig. 1 – to develop probabilistic surrogate SDOF models that represent a slew of MDOF models in which prevailing sources of model uncertainty are incorporated. In the first step, denoted as *Step* 1, multiple archetypes are designed based on the suggested conventional/relevant seismic codes. These archetypes may cover a wide range of practical designs representing buildings with a specific lateral load resisting system (e.g., SMFs). Index i is assigned to each archetype, i.e., $i \in \{1, 2 \ldots, N\}$ where N is the number of designed archetypes. *Step* 2 consists of conducting pushover analyses on MDOF models representing the archetypes designed in *Step* 1; for each archetype, M number of MDOF models, i.e., M realizations, are generated. Index j is assigned to each realization, i.e., $j \in \{1, 2 \ldots, M\}$. These realizations statistically represent the uncertainty in the component models of each archetype building. Altogether $N \times M$ models are generated and for each model, a pushover analysis using a load pattern consistent with the fundamental modal shape of the model is conducted. In *Step* 3, the force-displacement relationship of a surrogate SDOF model for each of the MDOF models in *Step* 2 is created using the results of the associated pushover analysis. In *Step* 4, the parameters of the force-displacement relationship of the $N \times M$ surrogate SDOF models generated in *Step* 3 are used to develop Bayesian regression models. These equations probabilistically describe surrogate model parameters as functions of building height. They can be used to generate random surrogate model realizations for probabilistic assessment of the collapse capacity of any building the design of which falls into the constraints used to generate the archetypes suggested in *Step* 1.

Implementation of *Step* 3 requires a defined procedure for the development of the force-displacement relationship for a surrogate SDOF model from the pushover curve of its corresponding MDOF model. This procedure is shown in Fig. 2 where the pushover curve associated with an MDOF and its surrogate SDOF model are illustrated. The pushover curve of the MDOF system relates the base shear of the structure to its roof displacement, shown with gray curve and axes. The force-displacement curve of the surrogate SDOF model, shown with dash curve and black axes, is generated by transforming the axes of the MDOF pushover curve using a factor denoted as Γ –see Eq. (1) – where m_k is the mass of k^{th} story, φ_k is k^{th} component of the fundamental mode shape normalized at the roof height, and N_s is the number of stories.

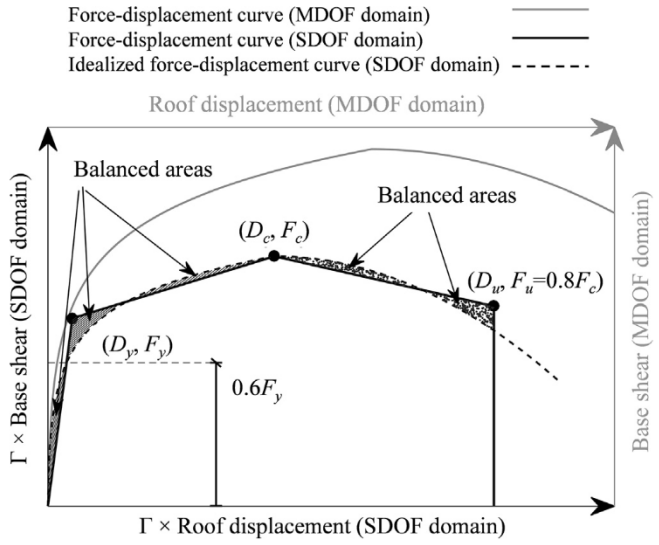

Fig. 2. Force-deformation idealization of the surrogate SDOF model.

The transformed force-displacement curve is then idealized with a multilinear backbone curve; see the solid black curve in Fig. 2. The point on the idealized curve denoted by pair (D_c, F_c) represents the instance where maximum strength is achieved. The yield point (D_y, F_y) is then obtained by applying two rules: i) balance among the areas confined between the idealized and the transformed force-displacement curves from zero to maximum strength, ii) the idealized and the transformed force-displacement curves sharing the same point at the strength level that equals to 60% of F_y. The ultimate deformation, D_u, is calculated by balancing the areas confined between the idealized and the transformed curves from maximum strength up to 20% drop in the maximum strength of the idealized force-displacement curve. Assuming that the dynamic response of the structure is mostly controlled by its fundamental mode of vibration, the period of the surrogate system is determined using Eq. (2), where m^* is the equivalent mass of the first mode of vibration of the MDOF system and is calculated according to Eq. (3).

$$\Gamma = \frac{\sum_{k=1}^{N_s} m_k \varphi_k}{\sum_{k=1}^{N_s} m_k \varphi_k^2} \tag{1}$$

$$T_1 = 2\pi \sqrt{\frac{m^* D_y}{F_y}} \tag{2}$$

$$m^* = \sum_{k=1}^{N_s} m_k \varphi_k \tag{3}$$

Parameters such as overstrength factor, Ω, ductility capacity, μ, maximum strength ratio, $\lambda_F{}^c$, pre-capping deformation ratio, $\lambda_D{}^c$, post-capping deformation ratio, $\lambda_D{}^u$, stiffness hardening ratio, α_s, and stiffness degrading ratio, α_c, can be determined from the suggested idealized backbone curve according to Eq. (4). Other parameters of the surrogate SDOF model, i.e., mass, m, and damping coefficient, ξ, are determined to represent the dynamic characteristics of the fundamental mode of vibration of the MDOF model. To clarify, m can be set arbitrarily so long as the period of the structure is set. In addition, ξ is set at the value of 0.03 so that it best describes the fundamental damping ratio of special steel moment frame buildings [34].

$$\Omega = \frac{F_c}{m^* S_{a,\text{Design}} g},\ \mu = \frac{D_c}{D_y},\ \lambda_F^c = \frac{F_c}{F_y},\ \lambda_D^c = \frac{D_c - D_y}{D_y},\ \lambda_D^u = \frac{D_u - D_c}{D_y},\ \alpha_s = \frac{k_s}{k_0},\ \alpha_c = \frac{k_{pc}}{k_0} \tag{4}$$

Where

$$k_0 = \frac{F_y}{D_y},\ k_s = \frac{F_c - F_y}{D_c - D_y},\ k_{pc} = \frac{F_c - F_u}{D_u - D_c},\ F_u = 0.8F_c \tag{5}$$

The hysteretic rule for the surrogate model should represent what is generally observed in the response of the MDOF structure to seismic excitation. In this study – and based on the available literature on the behavior of steel moment frames – we suggest using a peak-oriented hysteresis model [17]. Additionally, four cyclic deterioration modes are considered in this model, i.e., deterioration of the basic strength, post-capping strength, unloading stiffness, and reloading stiffness. Rates of cyclic deterioration are controlled by the rule that assumes the hysteretic energy-dissipation capacity is known and is independent of the loading history [35]. Based on this rule, the hysteretic energy-dissipation capacity of a system is defined as in Eq. (6), where E_t is the

Table 1
Design input variables.

Fixed Design Parameters	
Seismicity	D_{max}, S_s = 1.5, S_1 = 0.6
Soil type	D
Occupancy	Office
Material	ST52
Diaphragm	Rigid
Seismic framing system	Perimeter SMF
Design procedure	Response spectrum analysis
Live load (N/m^2)	2400
Partitions (N/m^2)	720
Exterior walls (N/m^2)	1200
Height of the first story	4.5 *m*
Height of other stories	3.5 *m*
Variable Design Parameters	
Ratio of gravity to seismic tributary area, $A_{gravity}/A_{seismic}$	0.167, 0.125, 0.100
Number of stories, N_s	3, 6, 9, 12, and 15
Span to height ratio, s/h	2.0, 1.5
Dead load (N/m^2), L_D	4309, 5267

hysteretic energy-dissipation capacity, F_yD_y, is twice the elastic energy at yielding, and γ is an adjustment factor whose suggested value is between 25 and 100 [17]. In this study, the proposed procedure is applied to steel SMF buildings. The details are described in the following sections.

$$E_t = \gamma F_y D_y \tag{6}$$

3. Building archetypes

Sixty steel SMF buildings are designed in accordance with modern seismic design codes [36–38]. The buildings are different in height, geometry, and gravity loading to reflect the practical range of design parameters. Table 1 shows the design variables for the building archetypes and their assigned values. The archetypes include buildings with 3, 6, 9, 12, and 15 stories; the first story height of each building is 4.5 m and all other stories are 3.5 m in height. Span to height ratio, s/h, gravity load, L_D, and the ratio of gravity to seismic tributary area, $A_{gravity}/A_{seismic}$, vary as suggested in Table 1. Different combinations of these three parameters (two values for s/h, two values for L_D, and three values for $A_{gravity}/A_{seismic}$) lead to 12 configurations for each building height. Plan views of the archetypes are shown in Fig. 3. In this figure, seismic frames are depicted with bold lines while gravity frames are shown in dash lines. Plan-1, Plan-2, and Plan-3 are associated with $A_{gravity}/A_{seismic}$ of 0.167, 0.125 and 0.1, respectively, in the east-west direction. A naming scheme with a format as N_s-a-b-c is introduced to define the archetypes. In this format, N_s shows the number of stories. a takes values of 1 and 2; 1 for s/h = 2 and 2 for s/h = 1.5. Similarly, b takes values of 1 and 2 for L_D = 4309 N/m^2 and L_D = 5267 N/m^2, respectively. Finally, c takes values of 1, 2, and 3, for Plan-1, Plan-2, and Plan-3, respectively.

Two-dimensional analytical models of MDOF structures are developed in Open System for Earthquake Engineering Simulation Platform (OpenSees) [39]. Partial resistance of gravity frames in the lateral behavior of the structure is also considered in the analytical models [40]. The nonlinear behavior of the structural systems is modeled using concentrated plasticity models. In this approach, beam-column elements are idealized with an elastic element and two plastic hinges at both ends. The panel zone is modeled as a rectangle composed of multiple rigid elements connected with hinges; a rotational spring at the upper right corner is added to capture the shear behavior of the panel zone [41]. It should be noted that all analytical models have some limitations. Referring to the models used in this study, real-time variations of axial-moment interaction and plastic hinge length are disregarded and the effect of axial force on moment capacity of column elements is approximately considered by reducing the moment capacity of column elements. The concept of structural idealization is illustrated in Fig. 4 for Plan-1. Due to symmetry in the plan of the structure, one seismic frame with half of the gravity frames, i.e., one out of two gravity frames in Plan-1, are considered in the analytical model.

Modified Ibarra-Medina-Krawinkler (IMK) hysteretic model [42] is used to capture the cyclic deterioration of plastic hinges. Fig. 5 shows the moment-rotation relationships of plastic hinges for SMF and gravity frames. The shape of the backbone curve for SMF elements is defined by six parameters; see Fig. 5(a): yield moment, M_y, ratio of peak to yield moment, M_c/M_y, residual moment, M_r, effective initial stiffness which is controlled by the modulus of elasticity, E_s, plastic rotation capacity, θ_p, and post-capping rotation capacity, θ_{pc}. The values for these parameters are determined based on the suggestion of [43] for monotonic behavior. Additionally, deterioration parameter, Λ, which defines the energy dissipation capacity for cyclic stiffness and strength deterioration is determined based on [44]. Beam-column connections in gravity frames are designed as conventional single-plate shear connections by considering a 30 mm gap between the beam end and the column face. A typical moment-rotation relationship for a plastic hinge in the gravity frames is shown in Fig. 5(b). AISC 341 [37] prohibits the placement of shear studs in protected zones. Therefore, beam-slab composite action at beam ends is arrested and moment-rotation relationship for beams are similar in positive and negative directions. For the panel zone spring, the tri-linear hysteretic behavior proposed by [45] is used.

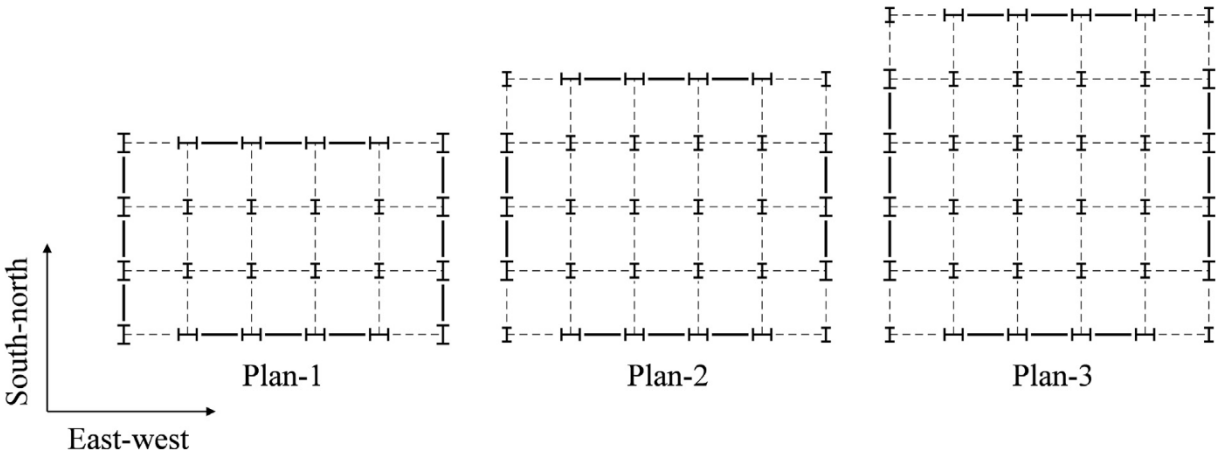

Fig. 3. Plan view.

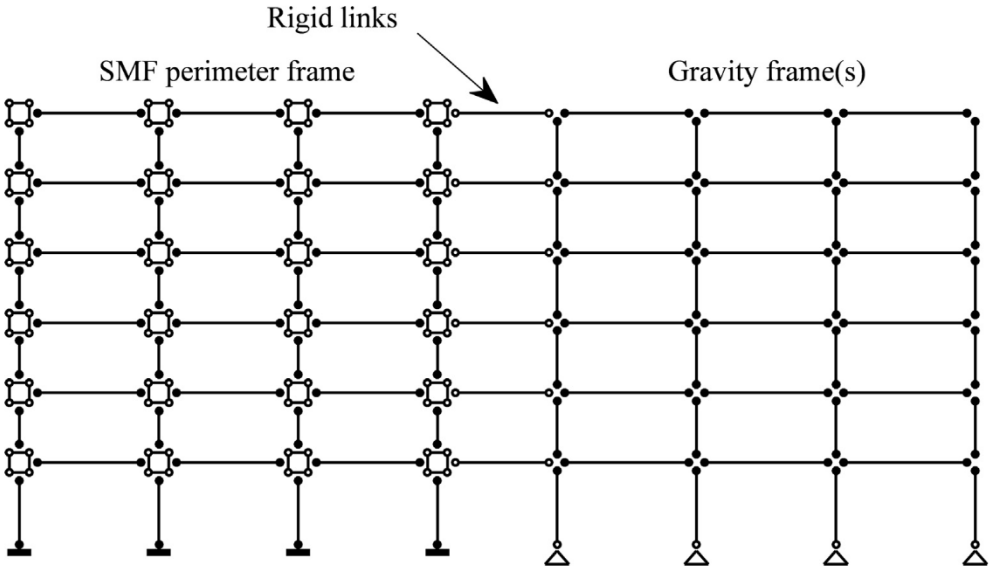

Fig. 4. Structural idealization.

4. Parameter uncertainties

The seven parameters defining the backbone curve of plastic hinges are considered as random variables. The statistical characteristics of these variables are obtained from test data for beam and column components [24,43]. In addition to hinge model parameters, modulus of elasticity and gravity loads are also treated as random variables. Dead load, L_D, is assumed to be normally distributed with a bias factor, i.e., ratio of mean to nominal value, of 1.05 and a coefficient of variation (CoV) of 0.1; live load, L_L, has a Gamma distribution with a bias factor of 1.00 and CoV of 0.25 [46,47]. Table 2 shows the CoV of all random variables.

In addition to the variability of each modeling parameter, the correlation between parameters is also taken into account in the uncertainty analysis. In this study, rotation and deterioration parameters within an element, i.e., intra-element, are assumed to be correlated; the correlation coefficients of these parameters are determined based on test data [48]. Moreover, a perfect correlation is assumed among similar parameters of different beam elements, i.e., inter-element. A similar assumption is made for parameters associated with column elements. This assumption is plausible as these elements are built by the same contractor and are likely to share similar behavior [2,50]. Table 3 shows the correlation coefficients among the parameters used in the modeling of MDOF systems in this study.

Table 2
Coefficient of variations of random variables.

Steel modulus of elasticity	E_s	0.05
Dead load	L_D	0.10
Live load	L_L	0.25
Plastic rotation of beam	$\theta_{p,b}$	0.30
Post-capping rotation of beam	$\theta_{pc,b}$	0.30
Plastic rotation of columns	$\theta_{p,c}$	0.39
Post-capping rotation of columns	$\theta_{pc,c}$	0.14
Residual strength of beams	$M_{r,b}$	0.00
Residual strength of columns	$M_{r,c}$	0.27
Cyclic deterioration of beams	Λ_b	0.36
Cyclic deterioration of columns	Λ_c	0.36
Yield moment of beams	$M_{y,b}$	0.10
Yield moment of columns	$M_{y,c}$	0.10
Peak moment of beams	$M_{p,b}$	0.10
Peak moment of columns	$M_{p,c}$	0.10

The Monte Carlo sampling method is employed to propagate the uncertainty in order to study the effect of model uncertainty on the global nonlinear behavior of SMF buildings. For this purpose, 5040 random realizations for each building height, i.e., 420 realizations times 12 building archetypes, are generated. This number of random

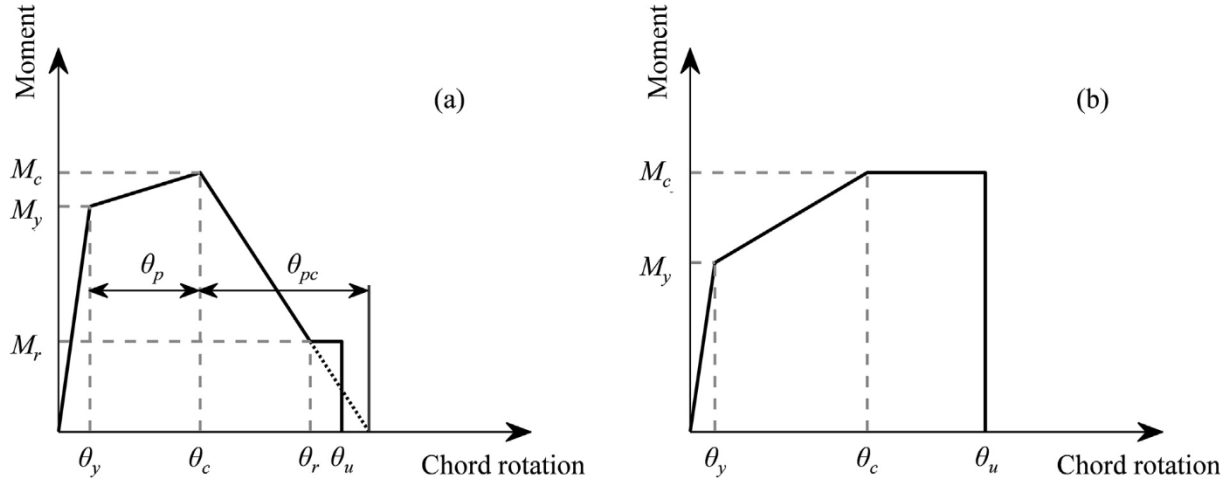

Fig. 5. Moment-rotation relationship for plastic hinges of (a) moment frame, and (b) gravity frame.

Table 3
Correlation coefficients between random variables.

	$\theta_{p,i}$	$\theta_{pc,i}$	Λ_i
$\theta_{p,i}$	1	0.69	0.44
$\theta_{pc,i}$	0.69	1	0.67
Λ_i	0.44	0.67	1

realizations is a minimum that leads to a standard error not larger than 2% in the estimation of the notable correlation coefficients between the parameters of the surrogate model, i.e., those that exceed 0.5 [49]. Pushover analysis is then conducted on a total number of 25,200 sampled models using a lateral load pattern proportional to the fundamental mode of vibration.

Fig. 6(a) and (b) show the results of pushover analyses of two archetypes, a 6-story building (6-1-1-1) and a 12-story building (12-1-1-1), respectively. The ordinates are normalized by the first mode equivalent mass of the structures, m^*. In these graphs, gray curves show the force-displacement relationships of the randomly generated frames. The black solid and dash lines show the median and the 16th and 84th percentiles of the results, respectively. The median of all pushover analyses for all archetypes are displayed in Fig. 6(c). This figure shows that the ductility capacity as well as the maximum normalized strength decrease when increasing the number of stories. The decrease in the ductility capacity stems from the significant P-Δ effect in taller buildings. As expected, taller buildings require lower design base shears, as shown in Fig. 6(c). More details on the distribution of pushover curves are presented in the next section.

5. Model inference

Force-displacement curves obtained from probabilistic pushover analyses are idealized to form the backbone curve of surrogate SDOF models. For each randomly sampled MDOF structure, one surrogate SDOF model is developed. Statistical analysis of parameters of surrogate SDOF models will guide the generation of closed-form equations to probabilistically describe the parameters of the surrogate SDOF model as functions of building height.

Recalling from previous sections, eight parameters are introduced in the multilinear backbone curve of the surrogate model shown in Fig. 2: T_1, Ω, μ, $\lambda_F{}^c$, $\lambda_D{}^c$, $\lambda_D{}^u$, α_s and α_c. We aim at selecting a subset of these parameters that uniquely define the backbone curve with no redundancy. To this aim, two parameters in *set*-1 = $\{\mu, \lambda_F{}^c, \lambda_D{}^c, \alpha_s\}$ and a single parameter in *set*-2 = $\{\lambda_D{}^u, \alpha_c\}$ are needed as a minimum, in addition to T_1 and Ω, to define the backbone curve of a surrogate model. Among the parameters in *set*-1, μ and $\lambda_D{}^c$ carry similar information; therefore, only one can be selected in the final set. We employ CoVs and correlations of the parameters as qualification indices to select the final set of defining parameters of the surrogate model. Fig. 7 shows the CoVs of parameters in *set*-1 and *set*-2. According to these figures, it is concluded that μ, $\lambda_F{}^c$, and $\lambda_D{}^u$ are the most stable parameters.

Correlations between all parameters of the equivalent model for buildings with 6 and 12 stories are presented in Table 4. The cells of the table are color-coded based on the value of the correlation coefficients such that a darker color indicates a higher correlation. It is observed that from *set*-1, μ and $\lambda_F{}^c$ have the lowest correlations compared with the other two parameters in this set. On the other hand, no obvious difference can be seen between the correlations of $\lambda_D{}^u$ and other parameters compared to α_c. The same conclusion can be made from the parameter correlations for other buildings. Considering both CoVs and correlations, T_1, Ω, μ, $\lambda_F{}^c$ and $\lambda_D{}^u$ are selected as the final set of input parameters for defining surrogate models. The statistical information of these parameters is presented in the following.

Fig. 8 shows the variation of surrogate model parameters for the considered range of SMF archetypes with the number of stories. For each parameter, boxplots correspond to the variation of each parameter in the range of 16th to 84th percentile. The solid black lines indicate the median of the fitted lognormal distribution from the 5040 data points. The dash lines indicate the range between the minimum and the maximum.

The far-left graph in Fig. 8 shows the variation of the fundamental period, T_1, with the number of stories, N_s. The observed relationship between T_1 and the building height, $H = 3.5(N_s - 1) + 4.5$, can be defined according to the following equation:

$$T_1 = 0.187H^{0.75} \tag{7}$$

This equation is plausible as it generates natural periods close to what is reported by Zareian et al. (2010) for an independent set of SMF archetypes. Fig. 8 shows that μ and $\lambda_D{}^u$ decrease as the structure height increases. This observation corroborates illustrations in Fig. 6(c) in which the nonlinear deformation capacity of the structure decreases by increasing the number of stories because of larger P-Δ effects. Another observation from Fig. 8 is that the overstrength factor, Ω, generally decreases as the building height increases. This observation is also corroborated in [51,52]. However, the change in Ω from 3-story to 6-story buildings does not follow this expected trend. To explain this

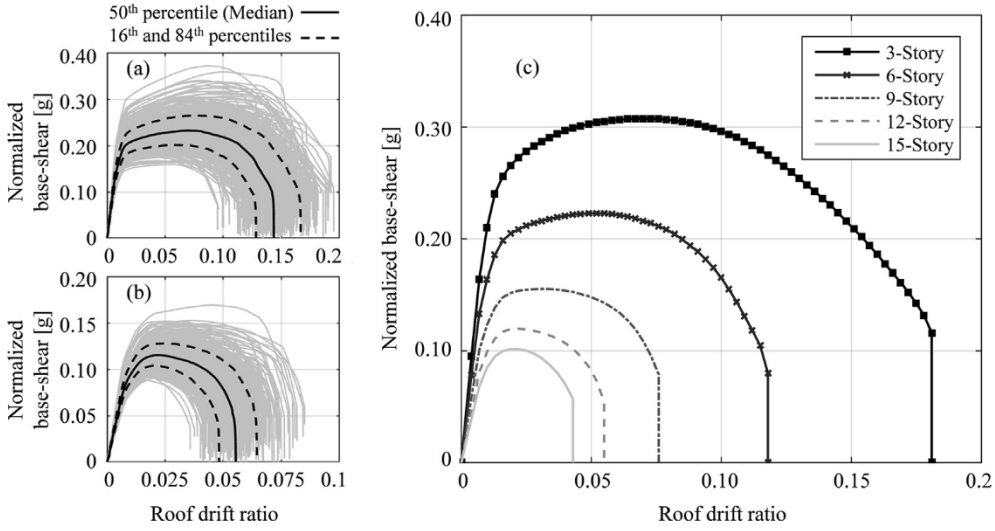

Fig. 6. Results of the probabilistic pushover analyses for (a) 6-story (6-1-1-1), (b) 12-story (12-1-1-1), and (c) median of all archetypes shown in the domain of the surrogate model.

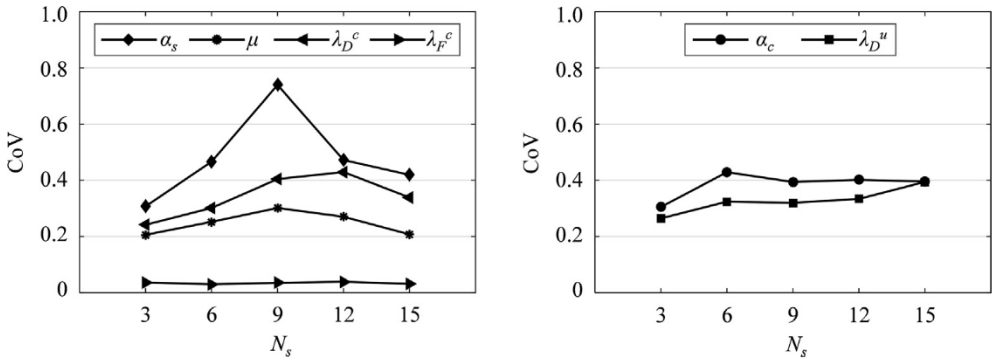

Fig. 7. Coefficients of variation of the surrogate model parameters.

Table 4
Coefficients of correlation between backbone parameters of the surrogate model.

	6-Story								12-Story							
	T_1	Ω	$\lambda_F{}^c$	μ	$\lambda_D{}^u$	$\lambda_D{}^c$	α_s	α_c	T_1	Ω	$\lambda_F{}^c$	μ	$\lambda_D{}^u$	$\lambda_D{}^c$	α_s	α_c
T_1	1.0	−0.8	−0.4	−0.3	−0.0	−0.3	0.1	−0.0	1.0	−0.8	0.4	−0.6	−0.4	−0.6	0.6	0.4
Ω		1.0	0.6	0.5	−0.1	0.5	−0.1	0.2		1.0	−0.4	0.6	0.3	0.6	−0.6	−0.3
$\lambda_F{}^c$			1.0	0.3	−0.0	0.3	0.3	0.1			1.0	−0.3	0.1	−0.3	0.6	−0.0
μ				1.0	−0.1	1.0	−0.7	0.1				1.0	0.4	1.0	−0.8	−0.5
$\lambda_D{}^u$		Sym.			1.0	−0.1	−0.0	−0.9		Sym.			1.0	0.5	−0.5	−0.9
$\lambda_D{}^c$						1.0	−0.7	0.1						1.0	−0.8	−0.5
α_s							1.0	−0.0							1.0	0.5
α_c								1.0								1.0

contradiction, it should be noted that two different drift limits are suggested for 3- and 6-story buildings. In ASCE 7-16 [38], a larger drift is allowed for buildings shorter than 5-story compared with taller ones, which can cause a smaller overstrength factor in a 3-story building compared to a 6-story building. As a final observation, we conclude that $\lambda_F{}^c$ is not dependent on the number of stories; therefore, it is considered as a constant for all building heights.

The probabilistic characterizations of surrogate model parameters are summarized in Table 5. In this table, medians and logarithmic standard deviations, $\sigma_{\ln}$, and correlation coefficients of the joint lognormal distributions of these parameters are provided. It has been shown that the lognormal distribution is a good representative of the distribution of structural modeling parameters [48]. Because $\lambda_F{}^c$ is almost constant for the entire range of the considered number of stories, the correlation of $\lambda_F{}^c$ with other parameters is disregarded. With the information presented in Table 5, the probabilistic surrogate model is determined given the number of stories. For number of stories other than the values reported in this study, one can find the medians of the model parameters by interpolation. However, determining the correlation coefficients and CoVs are not straightforward. To remedy, a prediction of the surrogate model parameters are given here in a Bayesian linear regression framework [53–55]. In particular, Ω, μ, and $\lambda_D{}^u$ are regressed against the fundamental period, T_1. For this purpose, the dataset consisting of 25,200 realizations of T_1, Ω, μ and $\lambda_D{}^u$ resulting from the idealization of pushover curves presented previously is employed. Multiple functional forms that included various transformations of the design parameters L_D, s/h and $A_{\text{gravity}}/A_{\text{seismic}}$, including linear and logarithmic, are examined. The examined functional forms are reduced through a stepwise model reduction [53], in which at every step, the regressor with the largest coefficients of variation is deemed inconclusive and eliminated from the model. Among all functional forms, the ones that best described the data and passed the statistical diagnostics test are as follows:

$$ln\mu = \theta_{0,1} + \theta_{1,1} ln T_1 + \varepsilon_1 \tag{8}$$

$$ln\lambda_D^u = \theta_{0,2} + \theta_{1,2} ln T_1 + \varepsilon_2 \tag{9}$$

$$ln\Omega^{'} = \theta_{0,3} + \theta_{1,3} ln T_1 + \varepsilon_3 \quad \text{where} \quad \Omega^{'} = \Omega \cdot S_{a,\text{Design}} \tag{10}$$

In these equations, $\theta_{j,i}$ and ε_i are model parameters and model errors, respectively. Bayesian linear regression yields the probability distribution of the model parameters and the model error [31] and

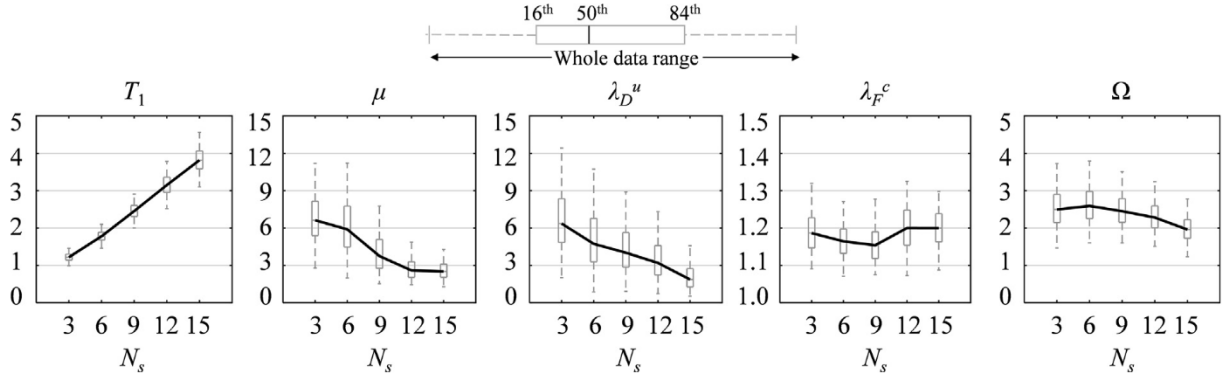

Fig. 8. Surrogate model parameters.

Table 5
Properties of the joint lognormal distribution of the surrogate model parameters.

		Median	$\sigma_{\ln}$	Coefficients of correlation			
				T_1	μ	$\lambda_D{}^u$	Ω
T_1	3-Story	1.22	0.06	1.0	−0.2	0.1	−0.8
	6-Story	1.78	0.06	1.0	−0.3	0.0	−0.8
	9-Story	2.45	0.06	1.0	−0.5	0.1	−0.8
	12-Story	3.15	0.06	1.0	−0.6	−0.4	−0.8
	15-Story	3.82	0.06	1.0	−0.3	−0.5	−0.8
μ	3-Story	6.62	0.20		1.0	−0.3	0.4
	6-Story	5.89	0.27		1.0	−0.1	0.5
	9-Story	3.75	0.30		1.0	0.0	0.5
	12-Story	2.60	0.24		1.0	0.5	0.6
	15-Story	2.52	0.21		1.0	0.4	0.3
$\lambda_D{}^u$	3-Story	6.35	0.27			1.0	−0.3
	6-Story	4.72	0.36			1.0	−0.2
	9-Story	4.01	0.34			1.0	−0.3
	12-Story	3.20	0.36			1.0	0.3
	15-Story	1.87	0.38			1.0	0.4
Ω	3-Story	2.50	0.15				1.0
	6-Story	2.60	0.14				1.0
	9-Story	2.46	0.13				1.0
	12-Story	2.29	0.13				1.0
	15-Story	1.96	0.13				1.0
$\lambda_F{}^c$	All	1.16	0.04	—			

Table 6
Second-moment statistics of the Bayesian regression models before the elimination of high correlations.

	Mean			CoV (%)			Correlation coefficients	
	μ	$\lambda_D{}^u$	Ω'	μ	$\lambda_D{}^u$	Ω'	$\theta_{0,i}$	$\theta_{1,i}$
$\theta_{0,i}$	2.18	2.11	−0.93	0.16	0.24	0.15	1.00	—
$\theta_{1,i}$	−0.97	−0.95	−1.00	0.40	0.59	0.14	−0.89	1.00
σ_{ri}	0.25	0.37	0.10	0.44	0.44	0.44		
R-Factor	0.84	0.73	0.97					

Table 7
Second-moment statistics of the Bayesian regression models after the elimination of high correlations.

	Mean				CoV (%)			
	μ	$\lambda_D{}^u$	Ω'	T_1	μ	$\lambda_D{}^u$	Ω'	T_1
$\theta_{1,i}$	−0.97	−0.95	−1.00	0.75	0.40	0.59	0.15	0.11
σ_{ri}	0.25	0.37	0.10	0.07	0.44	0.44	0.44	0.44
R-Factor	0.84	0.73	0.97	0.95				

hence, results in a probabilistic model for the backbone parameters. In particular, $\theta_{j,i}$ have a joint *t*-distribution and ε_i are normally distributed with zero means and standard deviations σ_{ri}. The second-moment statistics of model parameters and model errors are provided in Table 6. From this table, it is observed that in each model, the intercept, $\theta_{0,i}$, and the slope, $\theta_{1,i}$, are highly correlated. A high correlation between $\theta_{0,i}$ and $\theta_{1,i}$ indicates that these two explanatory parameters describe the same uncertainty and therefore, can be combined [53]. In other words, $\theta_{0,i}$ can be replaced by its conditional mean given $\theta_{1,i}$, as follows:

$$\theta_{0,i} = \mu_{\theta_{0,i}} + \rho_{\theta_{0,i}\theta_{1,i}} \frac{\sigma_{\theta_{0,i}}}{\sigma_{\theta_{1,i}}} (\theta_{1,i} - \mu_{\theta_{1,i}}) \tag{11}$$

Replacing Eq. (11) in Eqs. (8)–(10) leads to the following final model for predicting the backbone parameters:

$$ln\mu = +1.404 + \theta_{1,1}(lnT_1 - 0.80) + \varepsilon_1 \tag{12}$$

$$ln\lambda_D^u = +1.346 + \theta_{1,2}(lnT_1 - 0.80) + \varepsilon_2 \tag{13}$$

$$ln\Omega' = -1.817 + \theta_{1,3}(lnT_1 - 0.88) + \varepsilon_3 \text{ where } \Omega' = \Omega \cdot S_{a,\text{Design}} \tag{14}$$

A second round of Bayesian linear regression is performed with these reformulated functional forms, i.e., Eqs. (12)–(14). The second-moment statistics of the model parameters and model errors are shown in Table 7. The model successfully passes all the diagnostic tests of Bayesian linear regression. In particular, the model shows no sign of non-normality and heteroscedasticity of residuals. In addition, the CoV of the model parameters is very small, which indicates that the regressors are conclusive for this model [53]. With the proposed model, one can build the probabilistic surrogate model knowing the fundamental period of the system. If the fundamental period is not known, an approximation of T_1 can be determined using building height and the relationship given in Eq. (7).

Following the same procedure, the fundamental period of the structure can also be formulated in the Bayesian linear regression framework. To do so, T_1 is regressed against the total height of the structure, H. Eq (15) shows the resultant regression model that describes T_1 as a function of H. The second-moment statistics of the model parameters and model errors is shown in Table 7

$$lnT_1 = +0.704 + \theta_{1,4}(lnH - 3.18) + \varepsilon_4 \tag{15}$$

6. Validation

The validity of the proposed surrogate model in predicting the nonlinear response of SMF buildings is examined. The validation is assessed with two approaches. For this purpose, two 6- and 12-story building archetypes (6-1-2-1 and 12-1-2-1) are used, which has the following configurations; $s/h = 2$, $L_D = 5267$ N/m^2, and Plan 1. In the first approach, the collapse capacity of MDOF models is compared to that of surrogate models. To this end, incremental dynamic analyses (IDA) are conducted on two MDOF frames of 6 and 12 stories, and their surrogate models. IDA involves nonlinear time-history analysis of the structure with a set of ground motions increasingly scaled until collapse occurs [15]. In this assessment, the FEMA P-695 [56] set of 44 far-field ground motion records are utilized. Fig. 9 shows the pushover and the idealized backbone curve of the mean MDOF models for the two buildings in the domain of the surrogate models. The collapse capacity of the mean SDOF models are determined for three levels of cyclic

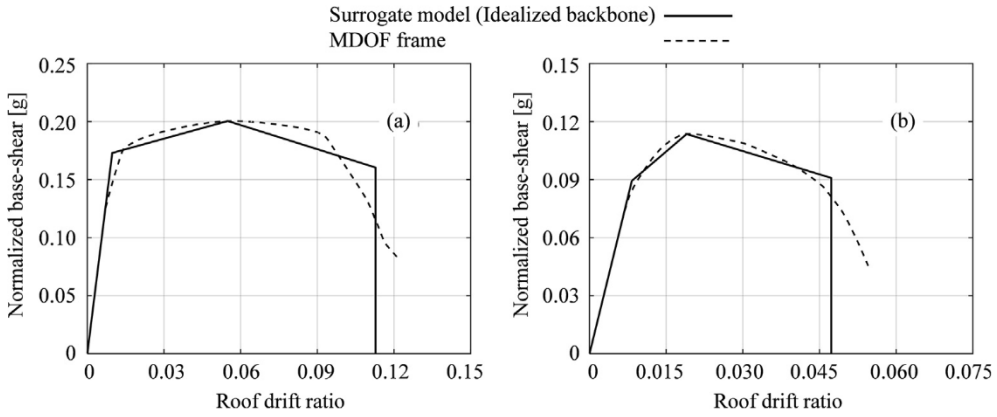

Fig. 9. Pushover results and the idealized backbone curves for (a) 6-Story (6-1-2-1) and (b) 12-Story (12-1-2-1) building in the domain of the surrogate model.

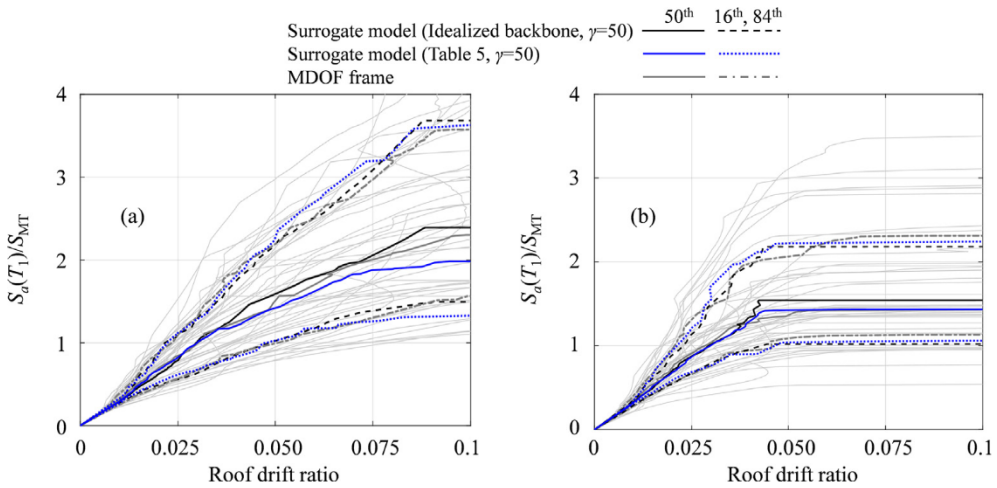

Fig. 10. IDA curves for (a) 6-Story (6-1-2-1) and (b) 12-Story (12-1-2-1) buildings.

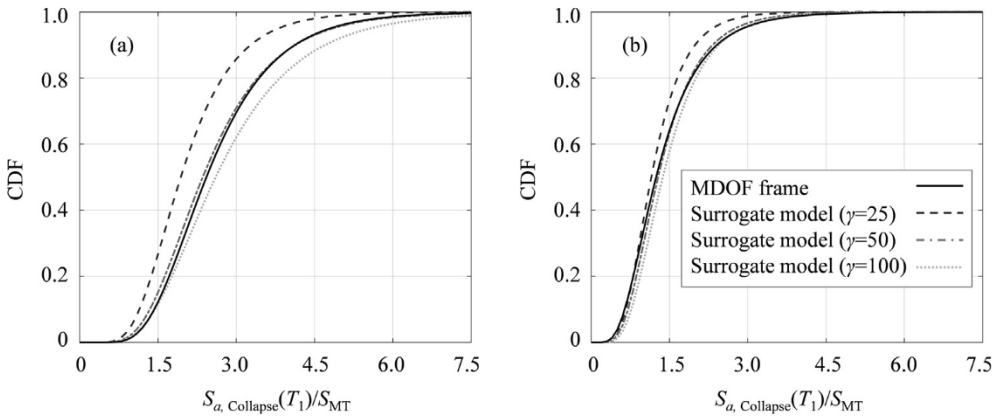

Fig. 11. Collapse capacity fragility curves for (a) 6-Story (6-1-2-1) and (b) 12-Story (12-1-2-1) buildings.

deterioration, as follows: slow, denoted by $\gamma = 100$; medium, denoted by $\gamma = 50$; and rapid, denoted by $\gamma = 25$ [17].

Fig. 10 compares the IDA results for the two MDOF frames and their surrogate models with medium cyclic deterioration, i.e., $\gamma = 50$. The first validation approach features surrogate models that are obtained directly from the pushover analysis of the associated MDOF frames, ignoring the uncertainty in the model parameters, to calibrate the level of cyclic deterioration for the surrogate model. For comparison, IDA analyses are also conducted in which the backbones are obtained from the median values shown in Rows 2, 4, 7, 9, 12, 14, 17, 19, and 21 of Table 5 for 6- and 12-story buildings. The results are reported with blue curves in Fig. 10. As seen, the use of the parameters suggested in Table 5 generates IDA curves that reasonably agree with those obtained from the direct pushover analysis of the MDOF frame. The ordinate in the plots of this figure represents the ratio of the spectral acceleration of the scaled ground motions to the spectral acceleration at the level of maximum considered earthquake, S_{MT}, for the seismic design category D_{max} in accordance with ASCE 7-16 [38], and the abscissa represents the roof drift ratio (RDR). In addition to the individual IDA curves for the MDOF frame shown by thin gray lines, the 16th, 50th, and 84th RDR percentiles are shown by thick gray and black lines for the MDOF and the surrogate systems, respectively. The percentiles are calculated

by ranking the drift data at multiple levels of normalized intensity measure, $S_a(T_1)/S_{MT}$. As illustrated in Fig. 10(a), given for instance at $S_a(T_1)/S_{MT}$ of 1.5, 16% of the records produce approximately drift ratios less than 0.032, 50% of the records drift ratios less than 0.05, and 84% of the records drift ratios less than 0.087. Comparison among the IDA percentiles of the MDOF and the surrogate systems indicate that the surrogate model closely mimics the roof drift ratios of the MDOF frames for the range of linear response to the collapse of the test structures.

Fig. 11(a) and (b) respectively show the cumulative density functions (CDF) of the collapse capacity obtained using MDOF frames, shown by solid lines, and the surrogate models with backbone curves obtained directly from the pushover curve of MDOF frames with three levels of cyclic deterioration for the 6- and 12-story buildings, shown by dash lines. Here, collapse capacity is defined as the scaled spectral acceleration at the fundamental period, S_a (T_1), normalized by S_{MT} at which IDA curve flattens to 10% of its initial slope, or roof drift exceeds 10%, whichever occurs first. It is observed from Fig. 11 that the surrogate model with medium cyclic deterioration is the one among three that best predicts the collapse capacity of the MDOF frame.

In the second validation approach, it is examined whether the probabilistic surrogate model can predict the roof drifts of MDOF frames considering both the RTR variability and the uncertainties in the structural model. For this purpose, buildings with same configurations as the ones used in the previous approach (archetypes 6-1-2-1 and 12-1-2-1) are utilized. For the uncertainty analysis, the Latin hypercube sampling method is utilized to generate ensembles of random MDOF and surrogate models. Using probabilistic characteristics of model parameters for MDOF and surrogate models provided in Tables 2, 3, and 5, 132 realizations are generated for MDOF and surrogate models for each of the 6- and 12-story buildings. In particular, parameters of surrogate models are generated according to the joint lognormal distribution with the statistics depicted in Table 5 for the 6- and 12-story buildings. Based on the results shown in Fig. 11, medium cyclic deterioration is considered for all surrogate models. The sampled model realizations are each matched randomly with one of the 44 ground motions of FEMA P-695, i.e., each ground motion is used three times. The procedure is repeated for several values of S_a (T_1), which represent multiple levels of seismic hazard. Shown in Fig. 12 are the resulting probability distributions of RDR for MDOF and surrogate systems at different hazard levels. In this figure, the probability density function (PDF) of RDR is shown in light and dark gray for MDOF and surrogate systems, respectively. The median RDR and the 16th and 84th percentiles are also displayed in Fig. 12 by solid and dash curves, respectively. The probability distributions and their statistics are obtained through a maximum likelihood analysis. In this analysis, a likelihood function is established by left-censoring the data points at RDR = 10% in accordance with [2]. That is, the likelihood function is the product of the PDF for the data points with RDR less than 10% and the complementary CDF of the data points with RDR larger than 10%. As such, the exact values of RDRs larger than 10% are not utilized when estimating the parameters of the distribution. To emphasize that the data points with RDR beyond 10% are left-censored, the corresponding area in Fig. 12(a) is colored with gray. As seen, not only the median, but also the 16th and 84th RDR percentiles obtained by the proposed surrogate model closely follow those of the MDOF frame. In addition, the distance between the 16th and the 84th percentiles is slightly wider for the proposed surrogate model compared to that of the MDOF frame. This indicates that the predictions of the proposed surrogate model are associated with more uncertainty, which is also reflected in the wider PDF of RDR obtained by this model. Hence, the proposed surrogate model correctly captures the additional uncertainties that are introduced in the prediction due to simplifying a detailed MDOF model into a surrogate SDOF model. Moreover, comparing the running time of the surrogate model with the MDOF frame shows a 95% reduction in the computational cost which corroborates the efficiency of the surrogate model. This amount of reduction in runtime is a rough estimate. As an example, on average, a nonlinear time history analysis of a 6-story MDOF moment frame model with average nonlinearity would take about 30 min while the same analysis using the proposed surrogate model takes about one minute. The proposed surrogate model has another advantage over the existing simplified models that estimate the building response, e.g., the capacity spectrum method and the underlying capacity curves proposed by FEMA-NIBS [9] in HAZUS. The latter approach relies on “average” capacity curves for a building type. For instance, FEMA-NIBS offers an average capacity curve for mid-rise steel moment frames. However, that curve actually belongs to a 5-story building, and it is hence assumed that all buildings that qualify as mid-rise steel moment frames follow the capacity curve of a 5-story frame. To remedy, one could produce a large library of fragility curves for various building heights and other parameters. In contrast, the proposed surrogate model can be utilized for a continuous range of parameters because intermediate cases can be regressed. In the final model that is proposed in this study, one building-to-building variability is explicitly considered in the surrogate model, and that is the building height. As mentioned before, the initial regression model included other regressors, i.e., various transformations of $A_{gravity}/A_{seismic}$, s/h, and L_D, that were deemed inconclusive through a model reduction process. Hence, these regressors were eventually discarded from the model and the resulting uncertainty was accounted for in the standard deviation of the model. The intention here is to illustrate the process and exercise it

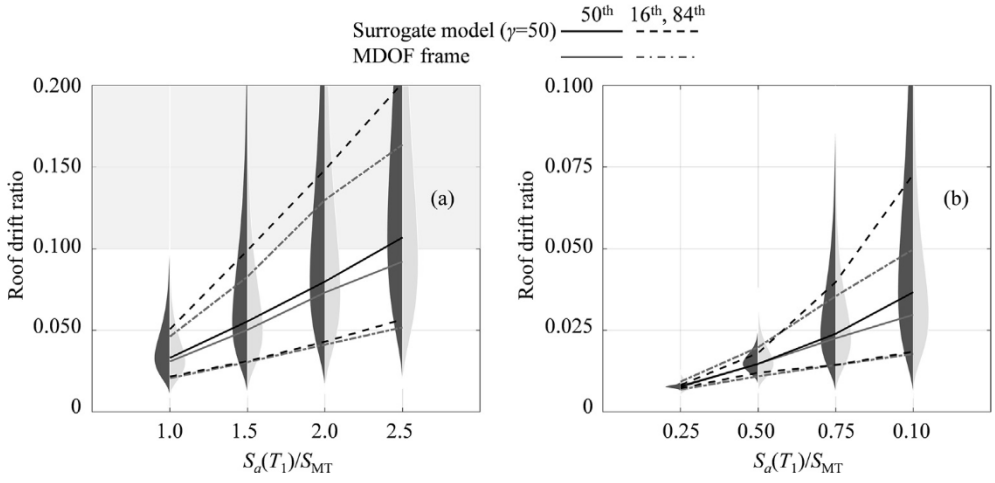

Fig. 12. Comparison of the 16th, 50th, and 84th percentile of roof drift ratios for MDOF and surrogate systems for (a) 6-Story (6-1-2-1) and (b) 12-Story (12-1-2-1) buildings.

for regular-in-plan and regular-in-height steel moment-resisting frames. Future research will address other parameters, such as material properties and irregularities.

7. Numerical example 1

The application of the suggested probabilistic surrogate model is explained in a low-rise building. For this purpose, a 4-story SMF building studied by Kazantzi et al. [57] is investigated. The building is designed for Los Angeles area and has a two-bay moment frame in the north-south direction. The first story of the building has a height of 4.6 m, and other stories are 3.7 m each. The fundamental period of the structure is calculated using Eq. (15), as follows:

$$T_1 = e^{+0.704+0.75(ln(4.6+3*3.7)-3.18)} = 1.47 \tag{16}$$

Using Eqs. (12)–(14) and the calculated fundamental period, median values of μ, ${\lambda_D}^u$, and Ω' are estimated as 6.07, 5.70, and 0.27, respectively. The median value for ${\lambda_F}^c$ is equal to 1.16 according to Table 5. By considering a unit mass for the surrogate model, other parameters of the system are computed, see Eqs. (17)–(19). In these equations, W is the weight of the surrogate model. IDA is performed using the same methodology as in [57], which employs an efficient incremental record-wise Latin hypercube sampling [58]. In this method, each model realization is paired with a single ground motion that is also randomly selected from a set of records. A sample of 320 realizations of the surrogate model is produced by randomly generating the parameters and the error term of the proposed Bayesian linear regression models that were previously presented in Table 7. A set of 60 ground motions were used in IDA. These are records on firm soil sites from events with a moment magnitude in the range of 6.5–6.7 and a distance to the fault rupture in the range of 13.3–31.7 km [59].

$$F_c = S_{a.\text{Design}}\Omega \cdot W = \Omega \cdot W = 0.27W,\ F_y = \frac{F_c}{\lambda_F^c} = \frac{0.27W}{1.16} = 0.23W \tag{17}$$

$$k_0 = \left(\frac{2\pi}{T_1}\right)^2 \frac{W}{g} = 18.15\frac{W}{g} \tag{18}$$

$$D_y = \frac{F_y}{k_0} = 0.13 \text{ m},\ D_c = \mu D_y = 0.75 \text{ m},\ D_u = D_c + \lambda_D^u = 1.46 \text{ m} \tag{19}$$

Fig. 13 compares the IDA curves of the MDOF frame as reported in [57] with the results of the proposed surrogate model. In this figure, black dash and solid lines represent the results from the IDA analysis of the original MDOF frame, while the gray lines show the results from IDA analysis of the surrogate model. In order to calculate the drift ratio of the surrogate systems, the displacement response of the model is divided by the effective modal height, $\bar{H} = 0.7H$. As observed in Fig. 13, the proposed surrogate model well predicts the behavior of the MDOF frame even though the data used to create the proposed model comes from MDOF frames with a different design than the one adopted here from [57] for comparison. In addition, the proposed surrogate model reduced the computational cost substantially, as was shown in the previous section.

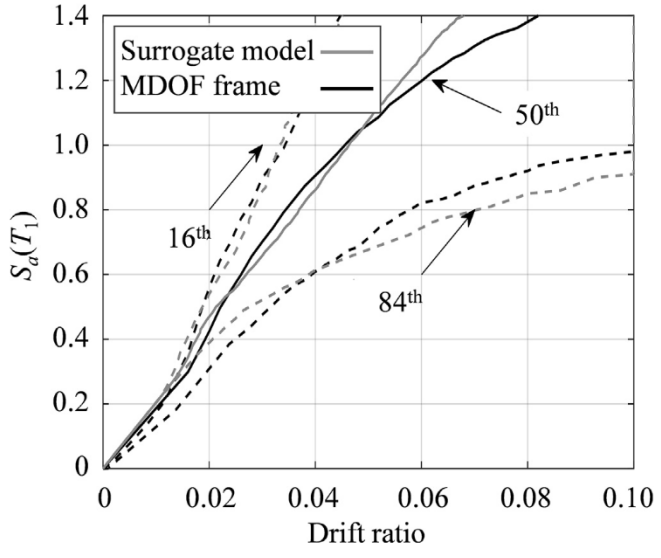

Fig. 13. Comparison of the IDA curves obtained by the proposed surrogate model and the MDOF frame in [57].

8. Numerical example 2

In this section, the proposed methodology is applied to a mid-rise building (i.e., 12-story) in which higher modes of vibration have a more pronounced effect on the seismic response. The structure was originally designed as a part of a NIST research project [52]. As the surrogate model represents SMF buildings designed according to the latest revisions of design codes, i.e., [36–38], the building is redesigned here to address the changes in the design codes. The plan configuration is shown in Fig. 14. In this figure, the bold lines indicate the moment frames that carry lateral forces. The height of the first story is 4.57 m, and the height of all other stories is 3.96 m. The gravity load consists of a uniformly distributed dead load of 4309 N/m^2 over each story, a cladding load of 1200 N/m^2 as a perimeter load, a live load of 960 N/m^2 on the roof, and a live load of 2400 N/m^2 on all other stories. Other design assumptions are in accordance with Table 1, which was presented previously. According to [38], the response modification factor, R, and the deflection amplification factor, C_d, are considered to be 8 and 5.5, respectively. The code-based period, T_{code}, calculated according to Section 12.8.2 of [38], is 2.25 s, which results in a seismic response coefficient, C_s, of 0.044. The member sizes for the redesigned moment frame in the east-west direction are summarized in Table 8. The analytical model for the redesigned building comprises moment frames and gravity frames in the east-west direction. The components of the system are modeled as previously described for the considered archetype buildings. The fundamental period of the analytical model is 3.18 s. Using Eqs. (12)–(15), the median values for the parameters of the surrogate model are calculated as follows (in accordance with Tables 7 and 5):

$$T_1 = e^{+0.704+0.75(ln(4.57+11\times3.96)-3.18)} = 3.4 \tag{20}$$

$$\mu = e^{1.404-0.97(lnT_1-0.8)} = 2.68 \tag{21}$$

$$\lambda_D^u = e^{1.346-0.95(lnT_1-0.8)} = 2.55 \tag{22}$$

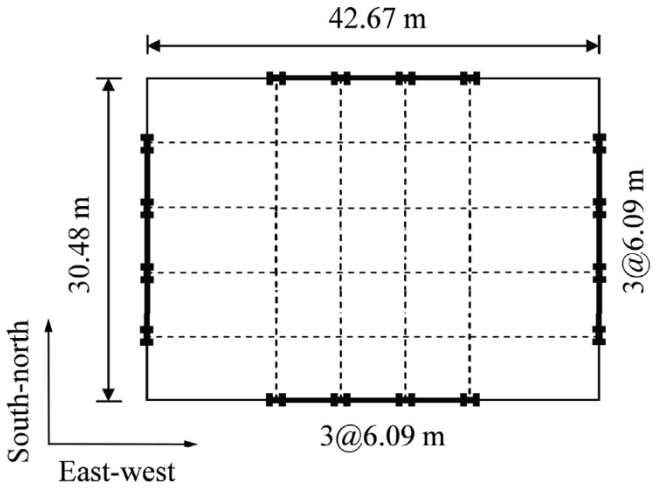

Fig. 14. Plan configuration of the 12-story building [52]

Table 8
Member sizes for the moment frame in east-west direction.

Story	Elevation (m)	Beam size	Exterior column size	Interior column size
12	48.13	24 × 84	24 × 94	24 × 131
11	44.17	24 × 84	24 × 94	24 × 131
10	40.21	27 × 94	24 × 94	24 × 162
9	36.25	27 × 94	24 × 131	24 × 162
8	32.29	27 × 114	24 × 131	24 × 207
7	28.33	27 × 114	24 × 146	24 × 207
6	24.37	27 × 114	24 × 146	24 × 207
5	20.41	30 × 116	24 × 192	24 × 229
4	16.45	30 × 116	24 × 192	24 × 229
3	12.49	30 × 116	24 × 250	24 × 229
2	8.53	30 × 116	24 × 250	24 × 229
1	4.57	30 × 116	24 × 306	24 × 229

$$\Omega^{'} = e^{-1.817-(lnT_1-0.88)} = 0.115 \tag{23}$$

$$\lambda_F^c = 1.16 \tag{24}$$

A sample of 44 realizations of surrogate model is produced by randomly generating the model parameters and the model error terms of the proposed Bayesian linear regression models that were previously presented in Table 7. For comparison, Fig. 15 shows the pushover curve of the analytical model along with cloud of randomly generated backbone curves of the surrogate model. The curves are plotted in the domain of surrogate model and the ordinate is normalized with the first mode equivalent mass of the structure, m^*.

The IDA analysis is conducted on the analytical model of the MDOF moment frame structure and the surrogate model considering both RTR variability and model uncertainty. For the IDA analysis, the 44 far-field record set of FEMA P-695 [56] is utilized, each randomly matched with the 44 randomly generated MDOF frames and surrogate models. Fig. 16 shows a summary of the IDA analyses. In this figure, light gray curves show the individual IDA curves for the MDOF structure. In addition, the 16th, 50th, and 84th percentiles of roof drift ratio are shown by thick gray and black lines for the MDOF and surrogate systems, respectively. The percentiles are calculated as described earlier. The drift ratio of the surrogate model is the ratio of the maximum displacement response of the model to the first modal height of the building. The reasonable agreement between the IDA results for MDOF and surrogate system suggests that the surrogate model estimates the roof drift ratios of taller buildings with an acceptable level of accuracy.

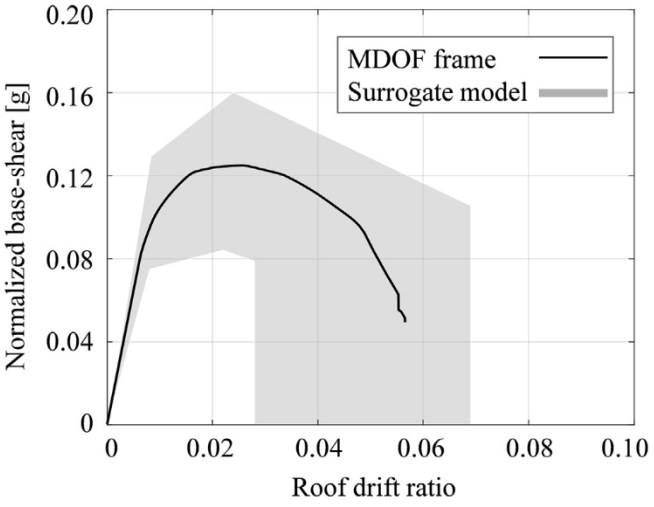

Fig. 15. Force-displacement relationship of the 12-story building and the cloud of randomly generated surrogate models shown in the domain of surrogate models.

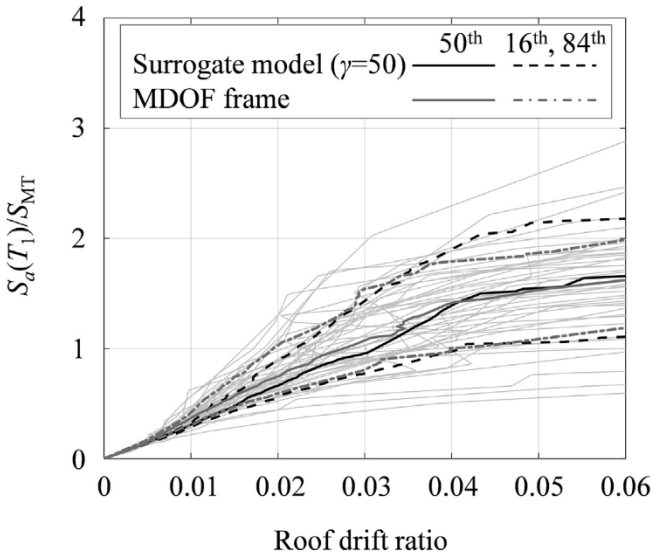

Fig. 16. Comparison of the IDA curves obtained by the proposed surrogate model and the 12-story MDOF frame.

9. Conclusion

This paper puts forward a novel methodology to develop a probabilistic surrogate SDOF model with multilinear backbone curve as a representative for MDOF systems. The proposed surrogate model proves to be an efficient substitution for the MDOF structure for probabilistic prediction of the roof drift ratio of the structure from the linearly elastic range through collapse. The proposed approach significantly alleviates the computational burden of large-scale seismic risk and resilience analyses and comprehensive parametric studies while exhibiting reasonable accuracy. To showcase the proposed methodology, 60 distinct SMF buildings, representing a practical range of design parameters and various numbers of stories, are designed. These buildings are then subjected to probabilistic pushover analyses to produce 25,200 realizations of pushover curves. An idealization method is introduced and employed to transform each pushover curve into one realization of the multilinear backbone curve of the surrogate model. Next, the resulting 25,200 backbone realizations are used to create Bayesian linear regression equations that predict the key parameters of the backbone curves given the fundamental period of the MDOF structure. The regression is naturally valid within the bounds of their underlying dataset, here, for plan-symmetric structures with periods in the range of $1 \sim 5$ s. The proposed model is validated by comparing the response statistics of detailed MDOF models and those of the corresponding surrogate models. The comparison shows that the proposed surrogate model can closely mimic the nonlinear behavior of the MDOF structures up to collapse. In addition, the IDA curves of an MDOF frame from the literature are compared against those obtained from the proposed model. The comparison proves that the proposed model well captures the behavior of the MDOF frame even though the studied structure is not from the test structures used to develop the surrogate model. The proposed methodology can be extended to other construction classes. Special attention to detail should be dedicated when applying the suggested methodology to other construction classes. For example, idealization of backbone curves for the surrogate model of, say, reinforced concrete shear wall structures, may require a deviation from what is used herein for steel moment frame structures. The hysteretic and damping model that best describes the general nonlinear behavior of the system would be another critical issue.

CRediT authorship contribution statement

Shaghayegh Vaseghiamiri: Methodology, Investigation, Writing - original draft, Software. **Mojtaba Mahsuli:** Conceptualization, Writing - review & editing, Supervision. **Mohammad Ali Ghannad:** Conceptualization, Writing - review & editing, Supervision. **Farzin Zareian:** Conceptualization, Writing - review & editing, Supervision.

Declaration of Competing Interest

The authors declare that they have no known competing financial interests or personal relationships that could have appeared to influence the work reported in this paper.

Acknowledgment

The authors thank the Ministry of Science, Research, and Technology of Islamic Republic of Iran whose graduate scholarship provided support for the lead author. The first three authors thank Iran National Science Foundation (INSF) for Grant No. 98012381 and Sharif University of Technology for Grant No. QA970110.

Appendix A. Supplementary material

Supplementary data to this article can be found online at https://doi.org/10.1016/j.engstruct.2020.110276.

References

[1] Eads L, Miranda E, Krawinkler H, Lignos DG. An efficient method for estimating the collapse risk of structures in seismic regions. Earthquake Eng Struct Dyn 2013;42:25–41.
[2] Gokkaya BU, Baker JW, Deierlein GG. Quantifying the impacts of modeling uncertainties on the seismic drift demands and collapse risk of buildings with implications on seismic design checks. Earthquake Eng Struct Dyn 2016;45:1661–83. https://doi.org/10.1002/eqe.2740.
[3] Borzi B, Pinho R, Crowley H. Simplified pushover-based vulnerability analysis for large-scale assessment of RC buildings. Eng Struct 2008;30:804–20.
[4] Fragiadakis M, Vamvatsikos D. Fast performance uncertainty estimation via pushover and approximate IDA. Earthquake Eng Struct Dyn 2010;39:683–703.
[5] Kosič M, Fajfar P, Dolšek M. Approximate seismic risk assessment of building structures with explicit consideration of uncertainties. Earthquake Eng Struct Dyn 2014;43:1483–502.
[6] ATC. NEHRP Guidelines for the Seismic Rehabilitation of Buildings. FEMA 273 1997; Redwood city, California.
[7] ASCE. Seismic Evaluation and Retrofit of Existing Buildings. ASCE/SEI 41-17 2017; Reston, Virginia.
[8] Mahaney JA, Paret TF, Kehoe BE, Freeman SA. The capacity spectrum method for evaluating structural response during the Loma Prieta earthquake. National Earthquake Conference: Earthquake Hazard Reduction in the Central and Eastern United States: A Time for Examination and Action, Memphis, Tennessee: US Central United States Earthquake Consortium (CUSEC); 1993, p. 501–10.
[9] FEMA-NIBS. Earthquake loss estimation methodology – HAZUS technical manual. Washington, DC: Federal Emergency Management Agency and National Institute of Building Sciences; 2003.
[10] Rossetto T, Gehl P, Minas S, Galasso C, Duffour P, Douglas J, et al. FRACAS: a capacity spectrum approach for seismic fragility assessment including record-to-record variability. Eng Struct 2016;125:337–48. https://doi.org/10.1016/j.engstruct.2016.06.043.
[11] Mahsuli M, Haukaas T. Seismic risk analysis with reliability methods, part I: Models. Struct Saf 2013;42:54–62.
[12] Mahsuli M, Haukaas T. Seismic risk analysis with reliability methods, part II: Analysis. Struct Saf 2013;42:63–74.
[13] Bernal D. Amplification factors for inelastic dynamic p–Δ effects in earthquake analysis. Earthquake Eng Struct Dyn 1987;15:635–51.
[14] Adam C, Ibarra L, Krawinkler H. Evaluation of P-delta effects in non-deteriorating MDOF structures from equivalent SDOF systems. In: 13th world conference on earthquake engineering, Vancouver, Canada; 2004. p. 15.
[15] Vamvatsikos D, Cornell CA. Incremental dynamic analysis. Earthquake Eng Struct Dyn 2002;31:491–514.
[16] Shi W, Lu X, Guan H, Ye L. Development of seismic collapse capacity spectra and parametric study. Adv Struct Eng 2014;17:1241–55.
[17] Ibarra L, Krawinkler H. Global collapse of frame structures under seismic excitations. College of Engineering University of California, Berkeley: Pacific Earthquake Engineering Research Center; 2005.
[18] ATC. Effects of Strength and Stiffness Degradation on Seismic Response. FEMA P440A 2009; Redwood city, California:312.
[19] Lee LH, Han SW, Oh YH. Determination of ductility factor considering different hysteretic models. Earthquake Eng Struct Dyn 1999;28:957–77.
[20] Pincheira J, Dotiwala FS, D'Souza JT. Seismic analysis of older reinforced concrete columns. Earthquake Spectra 1999;15:245–72.
[21] Ruiz-García J, Miranda E. Inelastic displacement ratios for evaluation of existing structures. Earthquake Eng Struct Dyn 2003;32:1237–58.
[22] Vian D, Bruneau M. Tests to structural collapse of single degree of freedom frames subjected to earthquake excitations. J Struct Eng 2003;129.
[23] Dolšek M, Fajfar P. Inelastic spectra for infilled reinforced concrete frames. Earthquake Eng Struct Dyn 2004;33:1395–416.
[24] Ibarra L, Krawinkler H. Variance of collapse capacity of SDOF systems under earthquake excitations. Earthquake Eng Struct Dyn 2011;40:1299–314. https://doi.org/10.1002/eqe.1089.
[25] Villar-Vega M, Silva V, Crowley H, Yepes C, Tarque N, Acevedo AB, et al. Development of a fragility model for the residential building stock in South America. Earthquake Spectra 2017;33:581–604.
[26] D'Ayala D, Meslem A, Vamvatsikos D, Porter K, Rossetto T, Crowley H, et al. GEM Guidelines for Analytical Vulnerability Assessment of Low/Mid-rise Buildings, Vulnerability Global Component Project; 2014.
[27] Shaghayegh Abtahi, Mojtaba Mahsuli, Ali Ghannad Mohammad. Probabilistic evaluation of strength demands for multistory shear buildings. J Struct Eng 2018;144:04018154. https://doi.org/10.1061/(ASCE)ST.1943-541X.0002153.
[28] Dolšek M. Simplified method for seismic risk assessment of buildings with consideration of aleatory and epistemic uncertainty. Struct Infrastruct Eng 2012;8:939–53.
[29] Peruš I, Klinc R, Dolenc M, Dolšek M. A web-based methodology for the prediction of approximate IDA curves. Earthquake Eng Struct Dyn 2013;42:43–60.
[30] De Bortoli M, Zareian F. Performance prediction equations for linear planar structural systems: concept, formulation, and validation. Earthquake Spectra 2017;34:697–718. https://doi.org/10.1193/110716EQS194M.
[31] Box GE, Tiao GC. Bayesian Inference in Statistical Analysis. Wiley Classics Library. Hoboken, New Jersey: Wiley-Inrerscience; 1992.
[32] Borekci M, Kirçil MS, Ekiz I. Collapse period of degrading SDOF systems. Earthquake Eng Eng Vibrat 2014;13:681–94.
[33] Khosravikia F, Mahsuli M, Ghannad MA. Probabilistic evaluation of 2015 NEHRP soil-structure interaction provisions. J Eng Mech 2017;143:04017065. https://doi.org/10.1061/(ASCE)EM.1943-7889.0001274.
[34] Bernal D, Döhler M, Kojidi SM, Kwan K, Liu Y. First mode damping ratios for buildings. Earthquake Spectra 2013;31:367–81. https://doi.org/10.1193/101812EQS311M.
[35] Rahnama M, Krawinkler H. Effects of soft soil and hysteresis model on seismic demands. John A. Blume Earthquake Engineering Center; 1993.
[36] AISC. Specification for Structural Steel Buildings. ANSI/AISC 360-10, Chicago, Illinois; 2010.
[37] AISC. Seismic Provisions for Structural Steel Buildings. AISC 341-16, Chicago, Illinois; 2015.
[38] ASCE. Minimum Design Loads and Associated Criteria for Buildings and Other Structures. Reston, VA: Structural Engineering Institute; 2017.
[39] MacKenna F, Fenves GL, Scott MH, Jeremic B. Open system for earthquake engineering simulation. Berkeley, CA: Pacific Earthquake Engineering Research Center; 2014.
[40] Wen R, Akbas B, Shen J. Practical moment–rotation relations of steel shear tab connections. J Constr Steel Res 2013;88:296–308.
[41] Gupta A, Krawinkler H. Seismic demands for the performance evaluation of steel moment resisting frame structures. Berkeley, CA: The John A. Blume Earthquake Engineering Center, Stanford University; 1998.
[42] Ibarra LF, Medina RA, Krawinkler H. Hysteretic models that incorporate strength and stiffness deterioration. Earthquake Eng Struct Dyn 2005;34:1489–511.
[43] Applied Technology Council. Guidelines for nonlinear structural analysis and design of buildings. part IIa - steel moment frames. Gaithersburg, MD: National Institute of Standards and Technology; 2017. https://doi.org/10.6028/NIST.GCR.17-917-46v2.
[44] Lignos D, Krawinkler H. Deterioration modeling of steel components in support of collapse prediction of steel moment frames under earthquake loading. J Struct Eng 2011;137:1291–302.
[45] Krawinkler H. Shear in beam Shear in beam-column joints in seismic design of steel frames. Eng J 1978;15:82–91.
[46] Nowak AS, Collins KR. Reliability of structures: reliability of structures. CRC Press; 2012.
[47] Nowak AS, Rakoczy AM. Uncertainties in the building process. Bull Polish Acad Sci 2013;61:129–35.
[48] Lignos D. Sideway collapse of deteriorating structural systems under seismic excitations. Stanford, CA: Stanford University; 2008.
[49] Bowley AL. The standard deviation of the correlation coefficient. J Am Stat Assoc 1928;23:31–4.
[50] Zareian F, Lignos DG, Krawinkler H. Evaluation of Seismic Collapse Performance of Steel Special Moment Resisting Frames Using FEMA P695 (ATC-63) Methodology, American Society of Civil Engineers; 2010. p. 1275–86.
[51] Jain Sudhir K, Rahul Navin. Seismic overstrength in reinforced concrete frames. J Struct Eng 1995;121:580–5. https://doi.org/10.1061/(ASCE)0733-9445(1995)121:3(580).
[52] NEHRP. Evaluation of the FEMA P-695 Methodology for Quantification of Building Seismic Performance Factors. NIST GCR 10-917-8, Redwood city, California; 2010.
[53] Gardoni P, Der Kiureghian A, Mosalam KM. Probabilistic capacity models and fragility estimates for reinforced concrete columns based on experimental

observations. J Eng Mech 2002;128:1024–38.
[54] Hossein Nasrazadani, Mojtaba Mahsuli, Hesam Talebiyan, Hamed Kashani. Probabilistic modeling framework for prediction of seismic retrofit cost of buildings. J Constr Eng Manage 2017;143:04017055.
[55] Aghababaei M, Mahsuli M. Component damage models for detailed seismic risk analysis using structural reliability methods. Struct Saf 2019;76:108–22.
[56] ATC. Quantification of Building Seismic Performance Factors. FEMA P695, Redwood city, California; 2009.
[57] Kazantzi AK, Vamvatsikos D, Lignos D. Seismic performance of a steel moment-resisting frame subject to strength and ductility uncertainty. Eng Struct 2014;78:69–77.
[58] Vamvatsikos D. Seismic performance uncertainty estimation via IDA with progresive accelerogram-wise Latin Hypercube sampling. J Struct Eng 2014.
[59] Vamvatsikos D, Sigalas I. Seismic performance evaluation of a horizontally curved highway bridge using incremental dynamic analysis in 3D. In: The 4th European workshop on the seismic behavior of irregular and complex structures, Thessaloniki, Greece; 2005.